Article

An ab Initio Study toward Understanding the Mechanistic Photochemistry of Acetamide

Xue-Bo Chen, Wei-Hai Fang, and De-Cai Fang

J. Am. Chem. Soc., **2003**, 125 (32), 9689-9698• DOI: 10.1021/ja029005h • Publication Date (Web): 19 July 2003

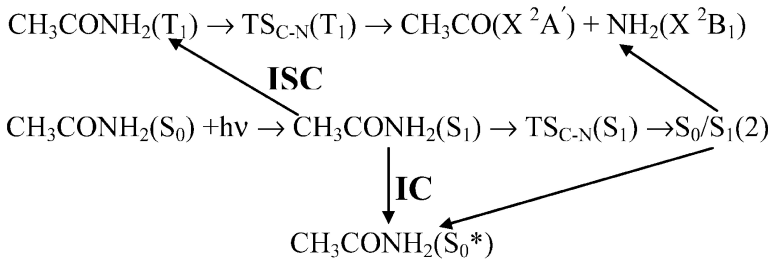

More About This Article

Additional resources and features associated with this article are available within the HTML version:

- Supporting Information
- Links to the 2 articles that cite this article, as of the time of this article download
- Access to high resolution figures
- Links to articles and content related to this article
- Copyright permission to reproduce figures and/or text from this article

View the Full Text HTML

J|A|C|S
ARTICLES
Published on Web 07/19/2003

An ab Initio Study toward Understanding the Mechanistic Photochemistry of Acetamide

Xue-Bo Chen, Wei-Hai Fang,* and De-Cai Fang*

Contribution from the Department of Chemistry, Beijing Normal University, Beijing 100875, People's Republic of China

Received October 18, 2002; E-mail: fangwh@bnu.edu.cn; dcfang@bnu.edu.cn

Abstract: The potential energy surfaces for CH_3CONH_2 dissociation into $CH_3 + CONH_2$, $CH_3CO + NH_2$, $CH_3CN + H_2O$, and $CH_3NH_2 + CO$ in the ground and lowest triplet states have been mapped with DFT, MP2, and CASSCF methods with the cc-pVDZ and cc-pVTZ basis sets, while the S_1 potential energy surfaces for these reactions were determined by the CASSCF/cc-pVDZ optimizations followed by CASSCF/MRSDCI single-point calculations. The reaction pathways leading to different photoproducts are characterized on the basis of the computed potential energy surfaces and surface crossing points. A comparison of the reactivity among $HCONH_2$, CH_3CONH_2, and $CH_3CONHCH_3$ has been made, which provides some new insights into the mechanism of the ultraviolet photodissociation of small amides.

1. Introduction

Proteins contain carbonyl, amino, and some other groups and can undergo numerous chemical reactions, of which the peptide bond formation and breakage have been of practical importance and fundamental interest. Knowledge of how the peptide bond interacts with ultraviolet light has important implications in many fields, such as laser surgery and photodegradation of polymers. As the simplest model molecules, the photolysis of formamide ($HCONH_2$), acetamide (CH_3CONH_2), and *N*-methylacetamide ($CH_3CONHCH_3$) has received much attention from the experimental viewpoint. Early in 1941, Volman[1] observed that CH_3CO and NH_2 were produced in aqueous photolysis of acetamide, while gas-phase photolysis of CH_3CONH_2 leads to the formation of CH_3, CO, and NH_2. At the temperature required for the gas-phase decomposition of CH_3CONH_2, the initially formed radicals such as CH_3CO and $CONH_2$ would undergo further decomposition. It was very difficult to distinguish the primary steps of the gas-phase decomposition of CH_3CONH_2 in this early study. Bosco and co-workers[2] used electron spin resonance spectroscopy to identify the free radicals produced in photolysis of formamide and acetamide. It was found that substitution of a methyl group on the nitrogen atom in $HCONH_2$ and CH_3CONH_2 does not change the mechanism of photolysis of peptide bonds, but it does have a little influence on the relative rate of different dissociation channels. The C−C and C−N bond cleavages were proposed as the primary channels for CH_3CONH_2 photodissociation

$$CH_3CONH_2 \rightarrow CH_3 + CONH_2 \quad (1)$$

$$\rightarrow CH_3CO + NH_2 \quad (2)$$

In addition to the radical reactions, direct molecular formation of $CH_3CN + H_2O$ and $CH_3NH_2 + CO$ was reported in the studies[3,4] of CH_3CONH_2 photolysis in solution and in the gas phase.

$$CH_3CONH_2 \rightarrow CH_3CN + H_2O \quad (3)$$

$$\rightarrow CH_3NH_2 + CO \quad (4)$$

Lundell and his partners have carried out matrix isolation FTIR studies[5] of the 193 nm-induced photodecomposition of formamide. In the Ar matrix, NH_3 and CO were found to be dominant products. However, the radical pair of $HCO + NH_2$ is initially formed in Xe matrixes, due to external heavy atom effects. Recently, Forde and Butler have made thorough studies[6,7] on the *N*,*N*-dimethylformamide photodissociation dynamics at 193 nm. The C−N bond cleavage was found to either proceed along the excited-state pathway leading to the products in the excited state or decay to a low energy state followed by formation of the fragments in the ground state.

Acetamide has long been of spectroscopic interest as a methyl-top molecule with a very low three-fold barrier and an equilibrium structure in which all of its atoms except for two of the methyl hydrogen atoms lie in the same plane.[8−12] A set of 115 rotational transitions in the torsional ground state have been fit to a model involving 28 torsion, rotation, and torsion−rotation interaction parameters to near experimental uncer-

(1) Volman, D. H. *J. Am. Chem. Soc.* **1941**, *63*, 2000.
(2) Bosco S. R.; Cirllo, A.; Timmons, R. B. *J. Am. Chem. Soc.* **1969**, *91*, 3140.
(3) Back, R. A.; Boden, J. C. *Trans. Faraday Soc.* **1971**, *69*, 88.
(4) Kakumoto, T.; Saito, K.; Imamura, A. *J. Phys. Chem.* **1985**, *89*, 2286.
(5) Lundell, J.; Krajewska, M.; Rasanen, M. *J. Phys. Chem. A* **1998**, *102*, 6643.
(6) Forde, N. R.; Butler, L. J. *J. Chem. Phys.* **1999**, *110*, 8955.
(7) Forde, N. R.; Butler, L. J. *Faraday Discuss.* **1997**, *108*, 221.
(8) Kitano, M.; Kuchitsu, K. *Bull. Chem. Soc. Jpn.* **1973**, *46*, 3048.
(9) Kydd, R. A.; Dunham, A. R. C. *J. Mol. Spectrosc.* **1980**, *69*, 79.
(10) Kojima, T.; Yano, E.; Nakagawa, K.; Tsunekawa, S. *J. Mol. Spectrosc.* **1985**, *112*, 494.
(11) Kojima, T.; Yano, E.; Nakagawa, K.; Tsunekawa, S. *J. Mol. Spectrosc.* **1987**, *122*, 408.
(12) Suenram, R. D.; Golubiatnikov, G. Y.; Leonov, I. I.; Hougen, J. T.; Ortigoso, J.; Kleiner, I.; Fraser, G. T. *J. Mol. Spectrosc.* **2001**, *208*, 188.

tainty.[12] The three-fold barrier to the torsion−rotation parameter in CH_3CONH_2 was predicted to be lower than 24 cm^{-1}. Five absorption bands have been identified for small amides,[13−15] a weak n → π^* transition at 210−230 nm, an intense $\pi \rightarrow \pi^*$ absorption below 169 nm, two Rydberg states at 185 and 159 nm, and a higher excited singlet state at 135 nm. The small amides have also been the subject of many other investigations, including the barrier to rotation about the C−N bond,[16] the structures[17,18] of the spectrum, the intramolecular H bond, and the relative stability of the isomers.[19,20] In addition, there have been many experiments in recent years to elucidate the resonance Raman spectra of small amides.[21−26]

Although the previous studies provide an invaluable starting point for further investigations of amides, there is a general lack of conclusive experiments on the primary reaction channels of the amide photodissociation. As far as we know, there are only a few ab initio studies that involve the potential energy surfaces of amide dissociation along the excited-state pathways. As a complementary of the experimental work, Lundell and his partners[5] have also carried out the CIS calculations of the potential energy surfaces for $HCONH_2$ decomposition into NH_2 + HCO in the low-lying electronic states. Because only the C−N bond distance was scanned with all other bond parameters kept at the ground-state equilibrium values, and because the CIS method is related to a limited inclusion of electron correlation, the CIS calculated potential energy surfaces are only qualitatively reliable. Butler and co-workers[6,7] have carried out an ab initio study of the S_1 structures at the CIS/6-31G* level, to better understand the nature of the $\pi \rightarrow \pi^*$ transition. In a previous letter,[27] we reported the CASSCF calculated potential energy surfaces for $HCONH_2$ decomposition.

The characterization of photodissociation reactions requires knowledge of more than one potential energy surface, including reaction pathways on different surfaces and the intersection regions where the system decays from one state to another. In comparison with thermochemical reactions, photochemical reactions are difficult to treat computationally. Robb, Olivucci, and Bernardi[28−31] have made great contributions to ab initio studies of molecular photochemistry. Mechanistic aspects of CH_3COCH_3, CH_2CHCHO, and $CH_2CHCOOH$ photodissociation[32−34] have been theoretically investigated in our previous work. With the general aid to understand peptide bond interaction with ultraviolet light, we are studying photodecomposition of a series of amides. In the present work, we mainly report high-level ab initio CASSCF and CASSCF/MRSDCI calculations of the potential energy surfaces for the CH_3CONH_2 dissociations in the low-lying electronic states. A comparison of the reactivity among $HCONH_2$, CH_3CONH_2, and $CH_3CONHCH_3$ provides some new insights into the photodissociation dynamics of small amides.

2. Computational Details

Stationary structures for $HCONH_2$, CH_3CONH_2, and $CH_3CONHCH_3$ in the lowest three electronic states have been fully optimized by means of the complete active space self-consistent field (CASSCF) method. The B3LYP and MP2 methods are also used to determine the structures in the ground (S_0) and lowest triplet (T_1) states. The cc-pVDZ and cc-pVTZ basis sets[35] are employed in the present investigation. Once convergence is reached, the harmonic frequencies are examined at this point to confirm the geometry obtained to be a true minimum or first-order saddle point. The optimization is terminated when the maximum force and its root-mean-square are less than 0.00045 and 0.0003 hartree/bohr, respectively. The CASSCF, DFT, and MP2 calculations reported here were carried out using the Gaussian 98 program package.[36]

The choice of the active space that is a crucial step for the CASSCF calculations cannot be regarded as completely solved to date. Most applications still involve some trial-and-error to select the proper orbitals. For the equilibrium geometries on the low-lying valence states, six electrons and four orbitals, originating from the C=O π and π^*, the oxygen nonbonding, and the $2p_z$ atomic orbital of the nitrogen atom (the $x-y$ plane is the molecular symmetry plane), are included in the active space. However, the dissociation process involves the C−C or C−N bond cleavage; the corresponding σ and σ^* orbitals should be used as the active orbitals. For a balanced description of the equilibrium geometries and transition state structures of the dissociations, we employed an active space of eight electrons in seven orbitals for the present CASSCF calculation, referred to as CAS(8,7). Besides the six active orbitals mentioned above, the seventh active orbital is determined by test calculations,[37] which is a valence orbital with antibonding character and is mainly localized on the C−C, C−O, and C−N regions.

(13) Basch, H.; Robin, M. B.; Kuebler, N. A. *J. Chem. Phys.* **1968**, *49*, 5007.
(14) Ballard, R. E.; Jones, J.; Read, D. A.; Inchley, M. *Chem. Phys.* **1998**, *147*, 629.
(15) Gingell, J. M.; Mason, N. J.; Zhao, H.; Walker, I. C.; Siggel, M. R. F. *Chem. Phys.* **1997**, *220*, 191.
(16) Bordwell, F. G.; Harrelson, J. A.; Lynch, T.-Y. *J. Org. Chem.* **1990**, *55*, 3337.
(17) Serrano-Andres, L.; Fulscher, M. P. *J. Am. Chem. Soc.* **1996**, *118*, 12190.
(18) Ottaviani, P.; Melandri, S.; Maris, A.; Paolo, G.; Caminati, W. *J. Mol. Spectrosc.* **2001**, *205*, 173.
(19) Manea, V. P.; Wilson, K. J.; Cable, J. R. *J. Am. Chem. Soc.* **1997**, *119*, 2033.
(20) Dickinson, J. A.; Hockridge, M. R.; Robertson, E. G.; Simons, J. P. *J. Phys. Chem. A* **1999**, *103*, 6938.
(21) Li, Y.; Garrell, R. L.; Houk, K. N. *J. Am. Chem. Soc.* **1991**, *113*, 5895.
(22) Li, P.; Chen, X. G.; Shulin, E.; Asher, S. A. *J. Am. Chem. Soc.* **1997**, *119*, 1116.
(23) Mayne, L. C.; Hudson, B. *J. Phys. Chem.* **1991**, *95*, 2962.
(24) Mayne, L. C.; Ziegler, L. D.; Hudson, B. *J. Phys. Chem.* **1985**, *89*, 3395.
(25) Markharn, L. M.; Hudson, B. S. *J. Phys. Chem.* **1996**, *100*, 2731.
(26) Song, S.; Asher, S. A.; Krimm, S.; Shaw, K. D. *J. Am. Chem. Soc.* **1991**, *113*, 1155.
(27) Liu, D.; Fang, W.-H.; Fu, X.-Y. *Chem. Phys. Lett.* **2000**, *318*, 291.
(28) Bernardi, F.; Olivucci, M.; Robb, M. A. *Chem. Soc. Rev.* **1996**, *25*, 321.
(29) Yamamoto, N.; Olivucci, M.; Celani, P.; Bernardi, F.; Robb, M. A. *J. Am. Chem. Soc.* **1998**, *120*, 2391.
(30) Ismail, N.; Blancafort, L.; Olivucci, M.; Kohler, B.; Robb, M. A. *J. Am. Chem. Soc.* **2002**, *124*, 6818.
(31) Blancafort, L.; Gonzalez, D.; Olivucci, M.; Robb, M. A. *J. Am. Chem. Soc.* **2002**, *124*, 6398.
(32) Liu, D.; Fang, W.-H.; Fu, X.-Y. *Chem. Phys. Lett.* **2000**, *325*, 86.
(33) Fang, W.-H. *J. Am. Chem. Soc.* **1999**, *121*, 8376.
(34) Fang, W.-H.; Liu, R.-Z. *J. Am. Chem. Soc.* **2000**, *122*, 10866.
(35) Dunning, T. H., Jr. *J. Chem. Phys*. **1989**, *90*, 1007. Woon, D. E.; Dunning, T. H., Jr. *J. Chem. Phys.* **1993**, *98*, 1358. Peterson, K. A.; Woon, D. E.; Dunning, T. H., Jr. *J. Chem. Phys*. **1994**, *100*, 7410.
(36) Frisch, M. J.; Trucks, G. W.; Schlegel, H. B.; Scuseria, G. E.; Robb, M. A.; Cheeseman, J. R.; Zakrzewski, V. G.; Montgomery, J. A.; Stratmann, R. E.; Burant, J. C.; Dapprich, S.; Millam, J. M.; Daniels, A. D.; Kudin, K. N.; Strain, M. C.; Farkas, O.; Tomasi, J.; Barone, V.; Cossi, M.; Cammi, R.; Mennucci, B.; Promelli, C.; Adamo, C.; Clifford, S.; Ochterski, J.; Petersson, G. A.; Ayala, P. Y.; Cui, Q.; Morokuma, K.; Malick, D. K.; Rabuck, A. D.; Raghavachari, K.; Foresman, J. B.; Cioslowski, J.; Ortiz, J. V.; Stefanov, B. B.; Liu, G.; Liashenko, A.; Piskorz, P.; Komaromi, I.; Gomperts, R.; Martin, R. L.; Fox, D. J.; Keith, T.; Al-Laham, M. A.; Peng, C. Y.; Nanayakkara, A.; Gonzalez, C.; Challacombe, M.; Gill, P. M. W.; Johnson, B. G.; Chen, W.; Wong, M. W.; Andres, J. L.; Head-Gordon, M.; Replogle, E. S.; Pople, J. A. *Gaussian 98*, revision A.3; Gaussian, Inc.: Pittsburgh, PA, 1998.

(37) The seventh active orbital was mainly determined by a criterion of the lowest energy. For example, the T_1 equilibrium geometry has been optimized with three different antibonding orbitals (mainly localized on the N−H, C−H, and C−CO−N regions, denoted by σ_1^*, σ_2^*, and σ_3^*, respectively) as the seventh active orbital. The CAS(8,7)/cc-pVDZ calculated energies are −207.92067, −207.92410, and −207.93051 au, respectively. In view of the calculated energy, we have chosen σ_3^* as the seventh active orbital and −207.93051 au as the energy of the T_1 equilibrium geometry. In addition, the CAS(8,7)/cc-pVDZ calculated one-electron density can give us some hints as to whether the chosen orbital is reasonable or not. If an antibonding orbital that is chosen as the active orbital can provide relatively low energy, generally, this orbital has relatively large one-electron density. In the above three calculations, one-electron densities on σ_1^*, σ_2^*, and σ_3^* are 0.003, 0.01, and 0.04, respectively. Similar test calculations were performed for the other stationary structures.

It should be pointed out that the σ or σ^* orbital in the active space is actually delocalized into the whole molecular backbone, but with remarkable bonding or antibonding character in the C−C and C−N regions. In a few instances (the S_0, T_1, and S_1 equilibrium structures and transition states of the T_1 and S_1 C−N bond cleavages), we used a larger active space of (10,8) for the CASSCF calculations. However, the obtained results showed that the (8,7) space is saturated, and the CAS(8,7) calculations allow us to capture the essential details relevant for description of the CH_3CONH_2 decompositions. We also attempted to optimize the stationary structures on the CH_3CONH_2 decarbonylation and dehydration pathways at the CAS(10,8) level with different active orbitals,[38] because two σ bonds may break simultaneously in these processes.

Because many of the valence electrons have been treated as filled closed-shell orbitals with no recovery of correlation energy, the present CASSCF calculations may overestimate the relative energies of the stationary structures on the T_1 and S_1 surfaces. In addition, the use of different active orbitals for equilibrium geometries and transition states makes some deviations in the calculated barrier heights. To refine the relative energies of the stationary structures, the single-point energy is calculated with the internally contracted MR-CI method that includes all single and double excitations relative to the CAS(8,7) reference wave functions (CASSCF/MRSDCI). A total of 24 valence electrons and all virtual orbitals are included in the MR-CI correlation calculations, with the C, N, and O 1s electrons treated as a frozen core. The MOLPRO program package[39] was used to perform the CASSCF/MRSDCI single-point energy calculations.

3. Results and Discussion

3.1. Reactions in the Ground State. A. The S_0 Equilibrium Structure. The structures of formamide ($HCONH_2$), acetamide (CH_3CONH_2), and *N*-methylacetamide ($CH_3CONHCH_3$) in S_0 have been fully optimized at the MP2, B3LYP, and CAS(8,7) levels with the cc-pVDZ and cc-pVTZ basis sets. The $-CO-NH_2$ group is predicted to be coplanar in the S_0 structures, but the methyl carbon deviates from the $-CO-NH_2$ plane by about 2° (the dihedral angle of N1−C2−O3−C4 is about 178°) in CH_3CONH_2 and $CH_3CONHCH_3$. The nonplanar structure is confirmed to be a minimum by frequency calculations. However, structural optimizations with the C_s symmetry constraint at the MP2 and B3LYP levels show that the C_s structure is 0.2−0.3 kcal/mol in energy lower than the nonplanar structure with the zero-point energy correction. Very recently, a set of rotational transitions have been fit to a model,[12] which provide a best estimation of 24 cm^{-1} for the barrier to the methyl rotation in CH_3CONH_2. The barrier is so low that it is very difficult to determine theoretically whether the C_s structure is a minimum or the quasi-C_s structure. In fact, planarity of the $-CO-NH-$ group is central to protein structure and function, which has been under strong debate.[40] Because we are concerned about the reaction processes in the present work, the C_s structures are used as the starting reactant, which will not have any significant influence on the relative energies of the other stationary structures.

Figure 1 shows the structure of CH_3CONH_2 in the ground state (S_0), along with the key bond parameters and atomic numbering. Because of the conjugation interaction between the nitrogen $2p_z$ and the C═O π electrons, the N1−C2 bond length is significantly short in comparison to a normal N−C single bond. Meanwhile, the hyperconjugation interaction between the methyl group and the −N−C═O moiety in CH_3CONH_2 makes the $2p_z$ and π electrons transfer toward the N and O atoms, respectively. This weakens a little the p−π interaction in the −N−C═O moiety. As a result, the N1−C2 bond is a little longer in CH_3CONH_2 (1.365 Å) than in $HCONH_2$ (1.357 Å). Because of the electron-donation nature of the CH_3 group, the methyl substitution on the N atom strengthens a little the p−π conjugation interaction in $CH_3CONHCH_3$.

B. The C−C and C−N Dissociation Energies. CH_3CONH_2 may dissociate into $CH_3 + CONH_2$ and $CH_3CO + NH_2$ along the ground-state pathways. We have made efforts to optimize a transition state for the C−C or C−N bond cleavage in the ground state, but optimizations always lead to the dissociation limit of $CH_3 + CONH_2$ or $CH_3CO + NH_2$. It is evident that no potential barrier above endothermicity exists on the S_0 pathway. The energy of the separated fragments was determined from a supermolecule optimization with the CAS(8,7)/cc-pVDZ approach, which is the same as that for the bound fragments. In this way, the C−C and C−N bond cleavages are predicted to be endothermic by 86.9 and 88.3 kcal/mol. The calculated C−N bond dissociation energy is close to the enthalpy change (90 kcal/mol) for the C−N dissociation of *N*,*N*-dimethylformamide.[6] Using heats of formation[41] at 0 K, we estimated the enthalpy of the reaction, $CH_3CONH_2 \rightarrow CH_3CO + NH_2$, to be 93 ± 2 kcal/mol. With the zero-point energy correction, the C−C and C−N dissociation energies become 80.5 and 82.2 kcal/mol, respectively, at the CAS(8,7)/cc-pVDZ level of theory.

C. Dehydration. Reaction 3, $CH_3CONH_2 \rightarrow CH_3CN + H_2O$, involves a breakage of the C═O double bond and the two N−H bonds, and formation of the two O−H bonds. It can be expected that the reaction would require more energy if it proceeds through a concerted mechanism. Thus, the concerted dehydration of CH_3CONH_2 is not investigated in the present work. A two-step process was determined for decomposition of CH_3CONH_2 into $CH_3CN + H_2O$. The first step is the H9 transfer from N1 to O3, producing an intermediate of $CH_3C(OH)═NH$, referred to as IM(S_0) hereafter. A four-centered transition state, TS1(S_0) in Figure 1, was found on the H9 transfer pathway. The barrier was predicted to be 40.5 and 42.5 kcal/mol by the B3LYP calculations with the cc-pVDZ and cc-pVTZ basis sets, respectively. The MP2/cc-pVDZ calculated value is 40.8 kcal/

(38) The C═O π and π^* orbitals, the O and N nonbonding orbitals, and the σ and σ^* orbitals of the C−C and C−N bonds are included in the active space for the CAS(10,8) optimization of the transition state of the decarbonylation reaction. For structural optimization of the transition state on the first step of the dehydration reaction, the C═O π and π^* orbitals, the σ and σ^* orbitals of the N−H and C−N bonds, and the O and N nonbonding orbitals are included in the (10,8) active space. In the optimization of the transition state on the second step of the dehydration reaction, the σ and σ^* orbitals of the N−H, O−H, and C−O bonds and the O and N nonbonding orbitals are used for the CAS(10,8) calculations.

(39) MOLPRO is a package of ab initio programs written by H.-J. Werner and P. J. Knowles, with contributions from Almlof, J.; Amos, R. D.; Cooper, D. L.; Deegan, M. J. O.; Dobbyn, A. J.; Eclert, E.; Elbert, S. T.; Hampel, C.; Lindh, R.; Lloyd, A. W.; Meyer, W.; Nicklass, A.; Peterson, K.; Pitzer, R.; Stone, A. J.; Taylor, P. R.; Mura, M. E.; Pulay, P.; Schutz, M.; Stoll, H.; Thorsteinsson, T.

(40) Fogarasi, G.; Szalay, P. G. *J. Phys. Chem. A* **1997**, *101*, 1400.

(41) Heats of formation for CH_3CONH_2, CH_3CN, and CH_3NH_2 are taken from: Frenkel, M.; Marsg, K. N.; Wilhoit, R. C.; Kabo, G. J.; Roganov, G. N. *Thermodynamics of Organic Compounds in the Gas State*; Thermodynamics Research Center: College Station, TX, 1994. Heats of formation for CO and H_2O are taken from: Cox, J. D.; Wagman, D. D.; Medvedev, V. A. *CODATA Key Values for Thermodynamics*; Hemisphere Publishing Corp.: New York, 1984. Heats of formation for CH_3CO, CH_3, and NH_2 are respectively taken from: Tsang, W. In *Energies of Organic Free Radicals*; Martinbo Simoes, J. A., Greenberg, A., Liebman, J. F., Eds.; Blackie Academic and Professional: London, 1996. Gurvich, L. V.; Veyts, I. V.; Alcock, C. B. *Thermodynamic Properties of Individual Substances*, 4th ed.; Hemisphere Pub. Co.: New York, 1989. Chase, M. W., Jr.; Davies, C. A.; Downey, J. R., Jr.; Frurip, D. J.; McDonald, R. A.; Syverud, A. N. JANAF Thermochemical Tables, 3rd ed. *J. Phys. Chem. Ref. Data* **1985**, *14, Suppl. 1*, 1.

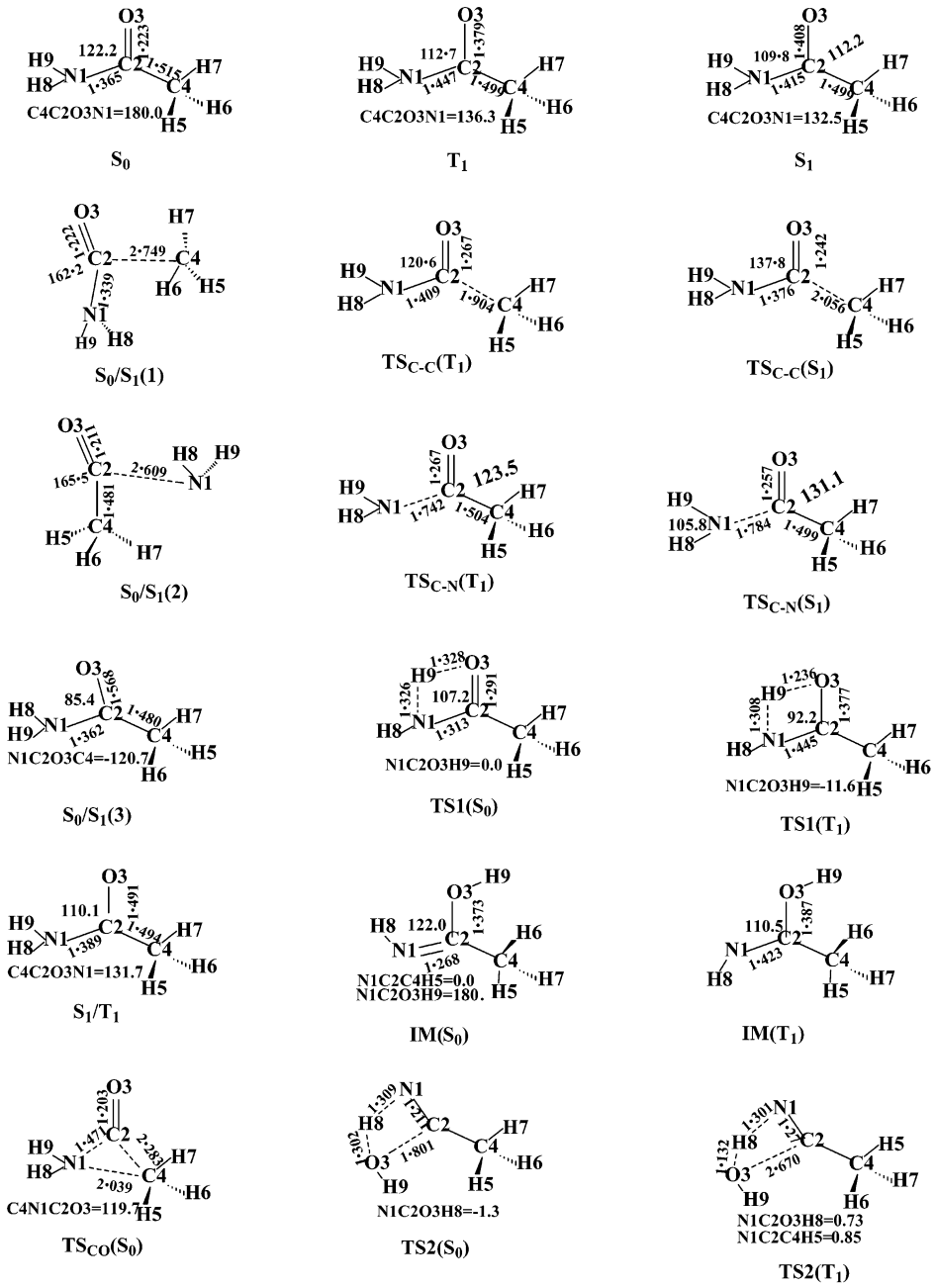

Figure 1. Schematic CH_3CONH_2 stationary structures on the S_0, S_1, and T_1 surfaces along with the key bond parameters (bond lengths in Å and bond angles in deg).

mol, close to the B3LYP/cc-pVDZ result. The second step has a four-centered transition state of $TS2(S_0)$, in which the H8 transfer is accompanied by the breaking of the C−O bond. The B3LYP/cc-pVDZ, MP2/cc-pVDZ, and B3LYP/cc-pVTZ calculations predict the barrier on the second step to be, respectively, 70.9, 69.5, and 71.2 kcal/mol with respect to the ground-state reactant, and 54.6, 54.2, and 54.9 kcal/mol with respect to the $IM(S_0)$ zero-level. The transition vectors associated with $TS1(S_0)$ and $TS2(S_0)$ are plotted in Figure 2a with the shown direction toward the corresponding products. The potential energy surface of the two-step process is shown in Figure 3, from which it can be concluded that the thermodehydration of CH_3CONH_2 takes place with difficulty at room temperature. The dehydration reaction of CH_3CONH_2 is endothermic by 13.6 and 24.1 kcal/mol at the MP2/cc-pVDZ and B3LYP/cc-pVDZ levels, respectively. The MP2 value is closer to the enthalpy of the reaction of 12.9 kcal/mol from heats of formation at 0 K.[41] As far as we know, dehydration reactions were not observed experimentally for $HCONH_2$ and $CH_3CONHCH_3$.

D. Decarbonylation. From the equilibrium structure of CH_3CONH_2, it can be expected that decarbonylation in the ground state is a concerted process. A three-centered transition state was determined by the B3LYP and MP2 optimizations, which is labeled as $TS_{CO}(S_0)$ hereafter. The optimizations with cc-pVDZ and cc-pVTZ basis sets give a similar $TS_{CO}(S_0)$ structure, in which the C4−C2, C4−N1, and C2−N1 distances are, respectively, 2.283, 2.039, and 1.471 Å at the B3LYP/cc-pVDZ level, and 2.306, 2.056, and 1.458 Å at the B3LYP/cc-pVTZ level. The C4−C2 bond is nearly broken, while the C2−N1 bond is slightly elongated in $TS_{CO}(S_0)$ with respect to

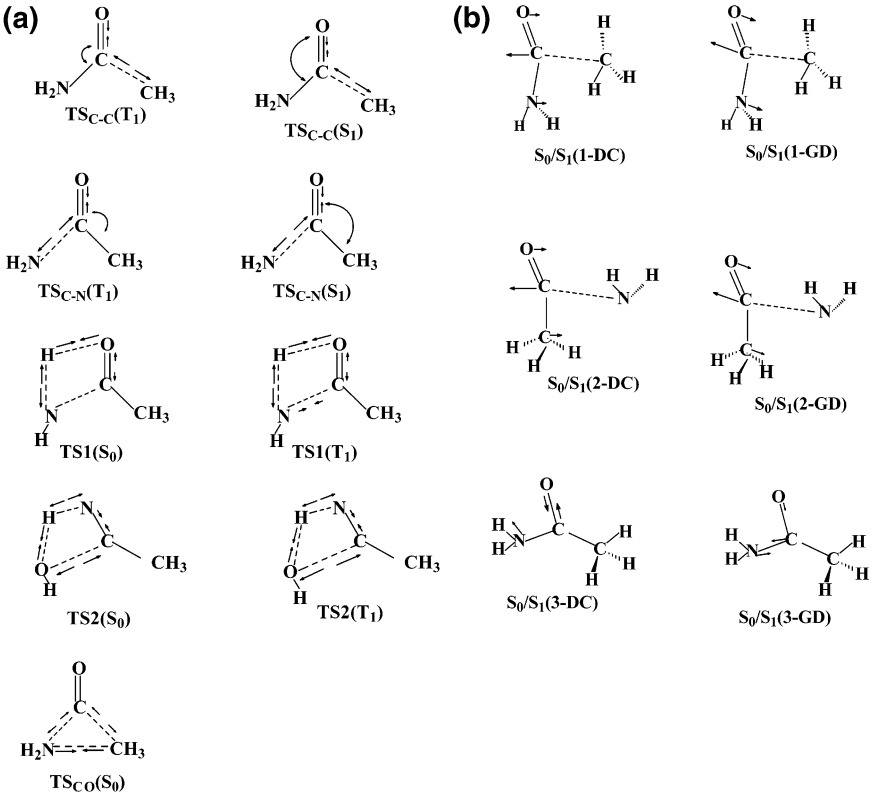

Figure 2. (a) Schematic transition vectors for the transition states with the shown direction toward the corresponding products; (b) schematic derivative coupling (DC) and gradient difference vectors at the three conical intersection points, $S_0/S_1(1)$, $S_0/S_1(2)$, and $S_0/S_1(3)$.

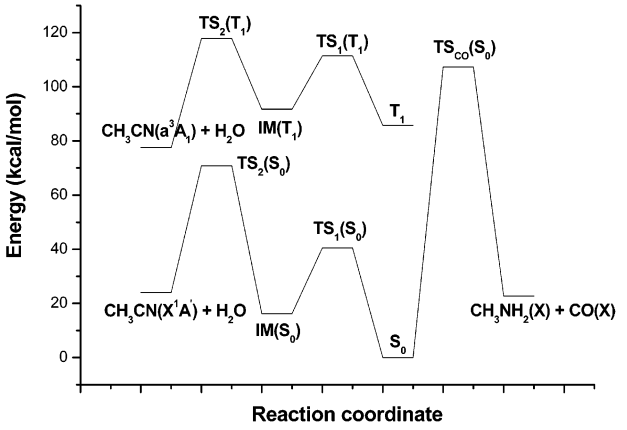

Figure 3. Schematic potential energy profiles for the dehydration and decarbonylation in the S_0 and T_1 states along with the B3LYP relative energies (kcal/mol).

those in the equilibrium structure of CH_3CONH_2. Starting from the $TS_{CO}(S_0)$ structure, the IRC calculations were performed at the B3LYP/cc-pVDZ level, which gives evidence that $TS_{CO}(S_0)$ is the transition state connecting CH_3CONH_2 and $CH_3NH_2 + CO$. The barrier to decarbonylation was calculated to be 107.2 kcal/mol at the B3LYP level with the two basis sets, which is 8.2 kcal/mol lower than that from the MP2/cc-pVDZ calculations. The B3LYP/cc-pVDZ calculations predict the barrier of decarbonylation to be 107.5 kcal/mol for $CH_3CONHCH_3$, which is nearly the same as that for CH_3CONH_2. The calculated results show that the S_0 decarbonylation proceeds with little probability for CH_3CONH_2 and $CH_3CONHCH_3$, due to a very high barrier on the pathway. The B3LYP/cc-pVDZ and MP2/cc-pVDZ calculations predict the decarbonylation reaction to be endothermic by 27.3 and 19.6 kcal/mol for CH_3CONH_2, close to the value of 23.8 kcal/mol obtained from heats of formation at 0 K.[41]

3.2. Reactions in the T_1 State. A. The T_1 Equilibrium Geometry. The T_1 equilibrium geometry of CH_3CONH_2 is optimized with the UMP2/cc-pVDZ and CAS(8,7)/cc-pVDZ methods. The resulting structure is shown in Figure 1 along with the CAS(8,7) bond parameters. In comparison with the equilibrium geometry in the ground state, the C−O and C−N bond lengths are significantly elongated in the T_1 structure. The most striking change is associated with the C4−C2−O3−N1 dihedral angle that is decreased from 180° in S_0 to 136.3° in T_1. A similar structural change from S_0 to T_1 was predicted by the UMP2/cc-pVDZ calculations. Natural orbital analysis clearly shows that the T_1 state originates from $n \rightarrow \pi^*$ excitation. One-electron excitation from n to π^* orbital leads to a partial breaking of the C═O π bond. As a result of this, the C−O bond is significantly elongated in T_1 with respect to that in S_0. From the viewpoint of the valence bond theory, the $n \rightarrow \pi^*$ excitation makes the C atom rehybridize from sp^2 in the ground state to sp^3 in the triplet state, resulting in the T_1 pyramidal equilibrium geometry. Similarly, the T_1 pyramidal equilibrium geometries were found for $HCONH_2$ and $CH_3CONHCH_3$. In fact, the T_1 state has a common pyramidal equilibrium geometry for a wide variety of aliphatic carbonyl molecules.[42−45] In addition, the $p-\pi$ conjugation between the N atom and the C═O group disappears in T_1, due to its pyramidal structure. This is the main

(42) King, R. A.; Allen, W. D.; Schaefer, H. F., III. *J. Chem. Phys.* **2000**, *112*, 5585 and references therein.
(43) Diau, E. W.-G.; Kotting, C.; Zewail, A. H. *ChemPhysChem* **2001**, *2*, 273; *ChemPhysChem* **2001**, *2*, 294 and references therein.
(44) Fang, W.-H.; Liu, R.-Z. *J. Chem. Phys.* **2001**, *115*, 10431.
(45) Chen, X.-B.; Fang, W.-H. *Chem. Phys. Lett.* **2002**, *361*, 473.

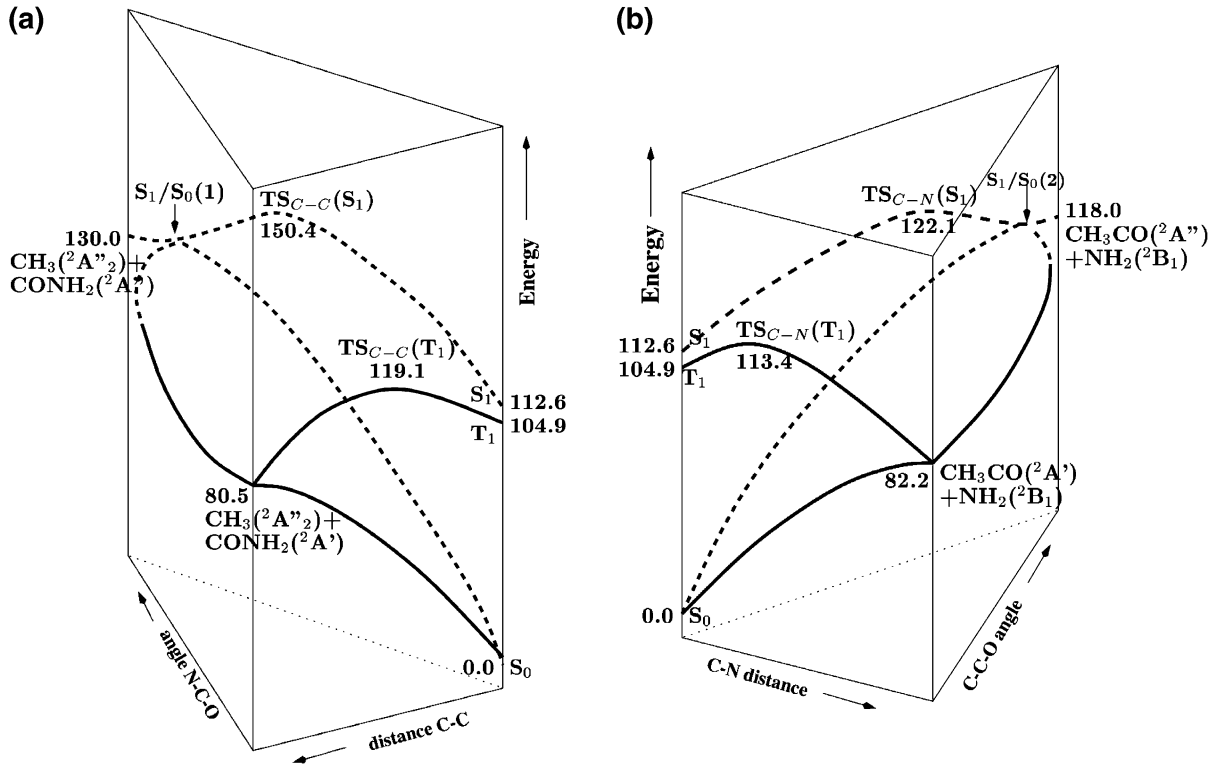

Figure 4. Schematic potential energy profiles for the C−C (a) and C−N (b) bond cleavages in the S_0, S_1, and T_1 states along with the CAS(8,7) calculated adiabatic excitation energies, barrier heights, and dissociation energies (kcal/mol).

reason the C−N bond is much longer in T_1 than that in S_0 for $HCONH_2$, CH_3CONH_2, and $CH_3CONHCH_3$.

B. The C−C Bond Fission. The ground-state radical of $CONH_2$ has $^2A'$ symmetry, and the methyl is an $^2A_2''$ species in the ground state. When the two ground-state fragments approach each other in C_1 symmetry, they can correlate with CH_3CONH_2 in the T_1 state. A transition state on the T_1 pathway, referred to as $TS_{C-C}(T_1)$ hereafter, was found and confirmed to be the first saddle point between $CH_3CONH_2(T_1)$ and $CONH_2$ ($X\ ^2A'$) + CH_3 ($X\ ^2A_2''$) by frequency calculations. At the CAS(8,7)/cc-pVDZ level, the C−C distance is 1.904 Å in $TS_{C-C}(T_1)$, which is 0.455 Å longer than that in the T_1 minimum. The UMP2/cc-pVDZ calculations predict the C−C distance to be increased by 0.349 Å from $CH_3CONH_2(T_1)$ to $TS_{C-C}(T_1)$. With respect to the vibrational zero-level of the T_1 state, the barrier height for the C−C bond fission on the T_1 surface is 14.2 at the CAS(8,7)/cc-pVDZ level, and it becomes 12.2 kcal/mol by the UMP2 calculations. The potential energy surfaces for the C−C bond cleavages are shown in Figure 4a, along with the CAS(8,7) relative energies. The barrier height of the T_1 C−H bond fission for $HCONH_2$ is 14.4 and 12.6 kcal/mol at the CAS(8,7) and UMP2 levels, respectively, which is nearly the same as that for CH_3CONH_2. The α C−C bond cleavage on the T_1 surface has a barrier of 13.6 and 12.5 kcal/mol at the corresponding level for $CH_3CONHCH_3$.

C. The C−N Bond Fission. Similar to the T_1 dissociation to $CONH_2$ (X^2A') + CH_3 ($X\ ^2A_2''$), the C−N fission reaction of $CH_3CONH_2 \rightarrow CH_3CO + NH_2$ can take place along the T_1 pathway, through the transition state of $TS_{C-N}(T_1)$. The CAS(8,7) calculations predict that the C−N distance is 1.742 Å in $TS_{C-N}(T_1)$, while this distance is predicted to be 1.694 Å by the UMP2 calculations. In addition, the C−N bond cleavage is accompanied by a large change of the relative orientation between the NH_2 and CH_3CO moieties, with the two groups nearly perpendicular to each other in $TS_{C-N}(T_1)$. A similar TS structure was found for the T_1 C−N bond fission of $HCONH_2$ or $CH_3CONHCH_3$. In the ground state, the C−N bond cleavage requires more energy than the C−C bond fission, due to the $p-\pi$ conjugation interaction. As pointed out before, this conjugation interaction is destroyed by the electron excitation from S_0 to T_1, and the C−N bond length is significantly elongated in the T_1 state. Qualitatively, the C−N bond dissociation proceeds easily from the T_1 states of $HCONH_2$, CH_3CONH_2, and $CH_3CONHCH_3$. Further evidence for this comes from the calculated barrier heights. The barrier to the C−N dissociation along the T_1 pathway is predicted to be 8.5 and 3.4 kcal/mol for CH_3CONH_2 at the CAS(8,7) and UMP2 levels of theory, respectively. The relatively small barrier on the C−N dissociation pathway predicts that the CH_3CONH_2 molecules undergo the C−N bond fission more easily than the C−C bond fission on the T_1 pathway. The barrier to the T_1 C−N dissociation is predicted to be 9.4 kcal/mol for $HCONH_2$ and 14.3 kcal/mol for $CH_3CONHCH_3$ at the CAS(8,7) level with the cc-pVDZ basis set. This barrier was respectively reduced to 4.3 and 0.5 kcal/mol by the UMP2/cc-pVDZ calculations.

D. Dehydration. It is possible for reaction 3, $CH_3CONH_2 \rightarrow CH_3CN + H_2O$, to proceed along the T_1 pathway. Like the dehydration in the ground state, a two-step process was determined for decomposition of CH_3CONH_2 into $CH_3CN + H_2O$ on the T_1 surface, which can be represented as $CH_3CONH_2(T_1) \rightarrow TS1(T_1) \rightarrow CH_3C(OH)NH(T_1) \rightarrow TS2(T_1) \rightarrow CH_3CN(T_1) + H_2O$. Both $TS1(T_1)$ and $TS2(T_1)$ are confirmed to be the transition states connecting $CH_3CONH_2(T_1)$ and the intermediate [$IM(T_1)$], and $IM(T_1)$ and $CH_3CN(T_1) + H_2O$, respectively. As

depicted in Figure 1, the bond parameters for TS1(T_1) and TS2(T_1) are quite different from those for TS1(S_0) and TS2(S_0), although TS1(S_0) and TS2(S_0) are also the four-centered transition states. The N1−C2 distance is 1.313 Å in TS1(S_0), while it is 1.445 Å in TS1(T_1) at the UB3LYP/cc-pVDZ level. TS1(S_0) leads to formation of IM(S_0) in which the N1═C2 is of double bond character. However, TS1(T_1) yields the triplet intermediate of IM(T_1), where N1−C2 is of single bond character. This is mainly responsible for a large difference in the N1−C2 distance between TS1(S_0) and TS1(T_1). The C2−O3 bond is partially broken in TS2(S_0) with a C2−O3 distance of 1.801 Å at the B3LYP/cc-pVTZ level, while this distance becomes 2.670 Å in TS2(T_1) by the UB3LYP/cc-pVDZ calculations. As a coproduct of T_1 dehydration, CH_3CN is in its triplet state that is 101.9 kcal/mol above the zero-level of the ground state. High endothermic character for the T_1 dehydration makes TS2(T_1) more productlike in structure. As shown in Figure 3, the first step has a barrier of about 26 kcal/mol at the UB3LYP level, which is nearly the same as that in the second step. Considering that these barriers are on the triplet pathways, they are not low. In fact, TS1(T_1) and TS2(T_1) have energies of about 120 kcal/mol with respect to the zero-level of the ground state. This predicts that the T_1 dehydration does not take place easily even with photoexcitation at a relatively short wavelength.

3.3. Reactions in the S_1 State. A. The S_1 Equilibrium Geometry. The S_1 equilibrium geometry of CH_3CONH_2 is optimized with the CAS(8,7)/cc-pVDZ approach. The resulting structure is shown in Figure 1, along with the key CAS(8,7)/cc-pVDZ bond parameters. The S_1 state also originates from the $n \rightarrow \pi^*$ excitation and has a pyramidal equilibrium geometry, which is similar to that for T_1. Yet there are some differences in the S_1 and T_1 bond parameters. The C−O bond length is 1.408 Å in S_1, while this bond length in T_1 is predicted to be 1.379 Å by the CAS(8,7)/cc-pVDZ optimizations. On the basis of the CAS(8,7) wave functions, Mulliken population analysis shows that the C and O atoms carry 0.14 and −0.17 atomic charges, respectively, in the T_1 state, while there are, respectively, 0.18 and −0.21 atomic charges distributed on the C and O atoms in the S_1 state. It is evident that the S_1 state has more C → O charge-transfer character than the T_1 state. This is the main reason that the C−O bond length is longer in S_1 than in T_1. Because there are more positive charges on the C2 atom in S_1 than in T_1, the lone-pair electrons on the N1 atom move toward the C2 atom. As a consequence, the N1−C2 bond is strengthened from T_1 to S_1, and the bond length is shortened from 1.447 Å in T_1 to 1.415 Å in S_1 at the CAS(8,7)/cc-pVDZ level. Analogous changes in structure from T_1 to S_1 were observed for $HCONH_2$ and $CH_3CONHCH_3$. The relatively strong N1−C2 bond in S_1 predicts that the N1−C2 bond dissociation takes place more difficultly along the S_1 pathway than on the T_1 surface.

B. The C−C Bond Fission. As pointed out before, the two ground-state radicals of $CONH_2$ ($X\ ^2A'$) and CH_3 ($X\ ^2A_2''$) can correlate with the S_0 and T_1 states of CH_3CONH_2. Qualitatively, the S_1 dissociation of CH_3CONH_2 leads to the fragments in an excited electronic state. A transition state on the S_1 pathway, referred to as $TS_{C-C}(S_1)$ hereafter, was found and confirmed to be the first saddle point by frequency calculations. The barrier height is predicted to be 37.8 kcal/mol at the CAS(8,7)/cc-pVDZ level with zero-point energy correction. On the basis of the CAS(8,7)/cc-pVDZ optimized structures, the single-point energies were calculated with the CASSCF/MRSDCI method, which reduces the barrier to 28.6 kcal/mol. The barrier to the C−C bond cleavage on the S_1 surface is much higher than that on the T_1 surface. The CASSCF/MRSDCI single-point calculations predict that the C−H and C−C bond dissociations have barriers of 29.6 and 28.9 kcal/mol along the S_1 pathway for $HCONH_2$ and $CH_3CONHCH_3$, respectively.

The C−C distance is 2.056 Å in $TS_{C-C}(S_1)$, which is 0.152 Å longer than that in $TS_{C-C}(T_1)$. In addition, the N1−C2−O3 angle is increased from 120.6° in $TS_{C-C}(T_1)$ to 137.8° in $TS_{C-C}(S_1)$. A large difference in the structure of $TS_{C-C}(T_1)$ and $TS_{C-C}(S_1)$ predicts that the two transition states connect the fragments in different electronic states. To determine the electronic state of the fragments produced by the S_1 C−C bond fission, IRC calculations have been carried out at the CAS(8,7)/cc-pVDZ level with the $TS_{C-C}(S_1)$ structure as the starting point. On one side, $TS_{C-C}(S_1)$ was confirmed to connect $CH_3CONH_2(S_1)$. However, on the other side, the problem of convergence was encountered during the state-specific CASSCF optimization of the IRC path with the C2−C4 separation at about 2.7 Å. Actually, the S_0 and S_1 states are close to each other in energy at this C2−C4 separation. A conical intersection between the S_1 and S_0 surfaces [$S_1/S_0(1)$] was found at the C2−C4 distance of 2.749 Å by the state-averaged CAS(8,7)/cc-pVDZ optimization. In addition to an increase of the C2−C4 distance, the N1−C2−O3 angle becomes 162.2° in the $S_1/S_0(1)$ structure, which is close to that of 179.8° in the first excited state of the $CONH_2$ radical. The $S_1/S_0(1)$ point is about 18.3 kcal/mol lower than $TS_{C-C}(S_1)$ in energy at the CAS(8,7)/cc-pVDZ level. The gradient difference and the derivative coupling vectors at this conical intersection point are depicted in Figure 2b. The derivative coupling vector corresponds to a N−C−O bending motion in the N1−C2−O3−C4 plane, which could lead to formation of either a hot parent molecule or the radical pair of CH_3 and $CONH_2$ in the ground state. However, the gradient difference vector corresponds to a N−C−O bending motion out of the N1−C2−O3−C4 plane, which mainly results in formation of the radical of $CONH_2$ in the excited state.

The conical intersection plays an important role in many nonadiabatic photochemical reactions. Because nonadiabatic decay through a conical intersection is very efficient, the decay from the upper to lower state usually occurs in a period of a single vibration.[28,43] The gradient difference and nonadiabatic coupling vectors at the $S_1/S_0(1)$ conical intersection show that the conical intersection could lead to formation of either a hot parent molecule or the fragments of $CONH_2$ ($X\ ^2A'$) + CH_3 ($X\ ^2A_2''$) in the ground state. Upon photoexcitation to the S_1 state, the C2−C4 bond cleavage starts from the Franck−Condon geometry on the S_1 surface, may relax to the S_1 minimum, overcomes the $TS_{C-C}(S_1)$ barrier, and then funnels through the $S_1/S_0(1)$ point down to either the fragments in the ground state or the hot parent molecule. The S_1 C−C bond dissociation can be represented as $CH_3CONH_2(S_1) \rightarrow TS_{C-C}(S_1) \rightarrow S_1/S_0(1) \rightarrow CONH_2\ (X\ ^2A') + CH_3\ (X\ ^2A_2'')$.

C. The C−N Bond Fission. Qualitatively, the CH_3CONH_2 molecules in S_1 may correlate adiabatically with the fragments of $CH_3CO + NH_2$ in the excited electronic state. A transition state, $TS_{C-N}(S_1)$, was found on the S_1 pathway by

the CAS(8,7)/cc-pVDZ calculations. The C−N bond fission has a barrier of 9.5 kcal/mol at the CAS(8,7)/cc-pVDZ level with zero-point energy correction. On the basis of the CAS(8,7)/cc-pVDZ optimized structures, the CASSCF/MRSDCI single-point energy calculations predict the barrier to be 7.6 kcal/mol with CAS(8,7)/cc-pVDZ zero-point energy correction. The same CASSCF/MRSDCI calculations give a barrier of 7.0 and 10.9 kcal/mol for the S_1 C−N bond cleavage of $HCONH_2$ and $CH_3CONHCH_3$, respectively. The barrier to the S_1 C−N dissociation is much lower than that for the S_1 C−C bond cleavage, but is a little higher than that for the C−N bond fission on the T_1 surface. The T_1 and S_1 potential energy surfaces for the C−C and C−N cleavages of CH_3CONH_2 are schematically depicted in Figure 4a and b, along with the CAS(8,7)/cc-pVDZ calculated relative energies.

The C−N distance is 1.784 Å in $TS_{C-N}(S_1)$, which is 0.369 Å longer than that in $CH_3CONH_2(S_1)$. The C4−C2−O3 angle is increased from 112.2° in the S_1 equilibrium geometry to 131.1° in $TS_{C-N}(S_1)$. The C−O bond length in $TS_{C-N}(S_1)$ is 1.257 Å, which is much longer than the length of the normal C═O double bond (1.223 Å at the CAS(8,7)/cc-pVDZ level). The CAS(7,7) calculations show that the CH_3CO radical in the first excited state ($^2A''$) has a linear C−C−O arrangement with a C−O bond length of 1.287 Å. Actually, the structure of the CH_3CO moiety in $TS_{C-N}(S_1)$ is closer to that of CH_3CO in the first excited electronic state. The H−N−H angle in $TS_{C-N}(S_1)$ is 105.8°, which is close to the corresponding value of 101° in the ground state ($^2B_1$) of the NH_2 radical, but is remarkably different from that in the first excited state ($^2\Pi$) of the NH_2 radical. Although the two excited states of the fragments, CH_3CO ($A\ ^2A''$) + NH_2 ($X\ ^2B_1$) and CH_3CO ($X\ ^2A'$) + NH_2 ($A^2\Pi$), are close to each other in energy, the structural features of $TS_{C-N}(S_1)$ predict that it connects CH_3CO (A^2A'') + NH_2 (X^2B_1) on the product side. The IRC calculations have been carried out at the CAS(8,7)/cc-pVDZ level with the $TS_{C-N}(S_1)$ structure as the starting point. On the reactant side, $TS_{C-N}(S_1)$ was confirmed to connect $CH_3CONH_2(S_1)$. However, on the product side, the problem of convergence was encountered during the state-specific CASSCF optimization of the IRC path. The S_1 and S_0 surface intersection, $S_1/S_0(2)$, was found at the N1−C2 distance of 2.609 Å by the state-averaged CAS(8,7)/cc-pVDZ optimization. The $S_1/S_0(2)$ intersection is 7.1 kcal/mol in energy above the S_1 minimum, but 4.2 kcal/mol lower than the top of the $TS_{C-N}(S_1)$ barrier at the CAS(8,7)/cc-pVDZ level. The C4−C2−O3 angle is increased from 112.2° in the S_1 equilibrium geometry to 131.1° in $TS_{C-N}(S_1)$ and to 165.5° in $S_1/S_0(2)$. The mechanism of the S_1 N1−C2 bond cleavage is similar to that for the S_1 C−C bond fission, which is represented as $CH_3CONH_2(S_1) \rightarrow TS_{C-N}(S_1) \rightarrow S_1/S_0(2) \rightarrow CH_3CO\ (X\ ^2A') + NH_2\ (X\ ^2B_1)$. It is also possible that the hot parent molecule can be formed after funneling through the $S_1/S_0(2)$ conical intersection.

As pointed out before, dehydration of CH_3CONH_2 involves stepwise hydrogen transfers. All attempts to search for a transition state on the first-step pathway of the S_1 dehydration were unsuccessful, duo to the problem of convergence encountered in the CAS(10,8) optimization. Instead, CIS calculations have been performed, which provides a barrier of 45.6 kcal/mol for the H9 transfer from N1 to O3 along the S_1 pathway. The CASSCF/MRSDCI single-point calculations on the CIS/cc-pVDZ optimized structures predict the barrier to be 31.2 kcal/mol. A relatively high barrier for the S_1 H9 transfer shows that S_1 dehydration is very difficult and is not in competition with S_1 C−N bond cleavage. Using different geometries as the initial guess, the CAS(10,8) optimizations of a concerted TS for the S_1 decarbonylation always converge to $TS_{C-C}(S_1)$. This shows that a concerted decarbonylation proceeds along the S_1 pathway with little probability. The stepwise mechanism for decarbonylation will be discussed in the following subsection.

3.4. Mechanistic Aspects. A. Adiabatic Excitation Energies. Experimentally, it has been established that the vertical excitation energies to the $^1n\pi^*$ (S_1) state are about 5.5 eV for several small amides.[13−15] This value was well reproduced by the CASPT2 calculations (5.54 eV for acetamide).[17] The present CASSCF/MRSDCI calculations give the $S_0 \rightarrow S_1$ vertical excitation energy of 5.8 eV for acetamide. As far as we know, the adiabatic excitation energies (0−0 energy gap) to the T_1 and S_1 state for CH_3CONH_2 were not reported in the literature to date. The adiabatic excitation energies from S_0 to the T_1 and S_1 were first calculated with the CAS(8,7)/cc-pVDZ approach, which gives the values of 104.9 and 112.6 kcal/mol for $S_0 \rightarrow T_1$ and $S_0 \rightarrow S_1$ transitions of CH_3CONH_2, respectively. The 0−0 energy gap between S_0 and T_1 is decreased to 101.7 kcal/mol by the MP2/cc-pVDZ calculations, while the 0−0 energy gap between S_0 and S_1 is predicted to be 106.8 kcal/mol by the CASSCF/MRSDCI single-point calculations on the basis of the CAS(8,7)/cc-pVDZ structures of the S_0 and S_1 states. The same CASSCF/MRSDCI calculations predict the 0−0 energy gap between S_0 and S_1 to be 104.6 and 104.3 kcal/mol for $HCONH_2$ and $CH_3CONHCH_3$, respectively. In comparison to the vertical excitation energy of 5.5 eV (126.8 kcal/mol) observed experimentally, the present calculations provide a reasonable description of the adiabatic excitation energies of $HCONH_2$, CH_3CONH_2, and $CH_3CONHCH_3$.

B. The T_1 and S_1 Surface Intersection. The geometry optimization for the T_1 and S_1 surface intersection (S_1/T_1) was carried out by searching for the lowest energy point of the two surface crossing seam. Slater determinants were used in the state-averaged CAS(8,7)/cc-pVDZ optimizations of the S_1/T_1 structure. The first observation is that the S_1/T_1 point is close to the S_1 minimum in structure. For example, the N1−C2, C2−O3, and C2−C4 bond lengths are, respectively, 1.389, 1.491, and 1.494 Å in S_1/T_1, and the corresponding values in S_1 are 1.415, 1.408, and 1.499 Å, respectively. The differences are small in bond angles and dihedral angles between S_1/T_1 and S_1. Actually, the S_1/T_1 structure comes from a deformation of the S_1 equilibrium geometry. With respect to the S_1 minimum, the S_1/T_1 intersection has an energy of 3.5 kcal/mol at the CAS(8,7)/cc-pVDZ level of theory. The structural similarity and small energy difference between S_1/T_1 and S_1 predict that intersystem crossing (ISC) from S_1 to T_1 may take place easily upon photoexcitation of CH_3CONH_2 to the S_1 state.

Here, we pay a little attention to the possibility of $S_1 \rightarrow T_2$ intersystem crossing in photodissociation processes of CH_3CONH_2. The T_2 structure was optimized at the CAS(8,7)/cc-pVDZ level with a C_s symmetry constraint. The T_2 state was confirmed to be of $^3\pi\pi^*$ character by natural orbital analysis on the CAS(8,7) wave functions. The two singly occupied orbitals can be approximately represented as $0.42\ 2p_z(N) - 0.45\ 2p_z(C) - 0.85\ 2p_z(O)$ and $0.51\ 2p_z(N) - 0.95\ 2p_z(C) + 0.75$

$2p_z$(O), respectively. However, the T_2 state is 16.7 kcal/mol higher than the S_1 minimum in energy and 123.5 kcal/mol above the S_0 minimum at the CASSCF/MRSDCI level. The CASPT2 calculations by Serrano-Andres and Fulscher[17] predicted the vertical excitation energy to T_2 to be 5.57 eV (128.4 kcal/mol), which is a little higher than that to the S_1 state. It has been found experimentally that the initial dephasing out of the S_1 Franck−Condon (FC) region occurs in less than 50 fs for a series of aliphatic ketones.[43] Because the T_2 state is energetically higher than the S_1 state in the FC region and relaxation from the S_1 FC geometry is very fast, the $S_1 \rightarrow T_2$ ISC is expected to occur with less probability upon photoexcitation to the S_1 state of CH_3CONH_2. If the molecules are promoted to the S_2 or higher excited state by photoexcitation at a short wavelength, the T_2 state probably plays an important role in dissociation mechanisms.

C. The S_1 and S_0 Surface Intersection in the Franck−Condon Region. Structural optimization of the S_1 and S_0 surface intersection was further carried out by searching for the lowest energy point of the surface crossing seam at the state-averaged CAS(8,7)/cc-pVDZ level. The obtained structure, referred to as $S_1/S_0(3)$, is shown in Figure 1 along with its key bond parameters. The C−O and C−N distances are, respectively, 1.568 and 1.362 Å in the $S_1/S_0(3)$ structure, which are different from the corresponding values of 1.408 and 1.415 Å in the S_1 equilibrium geometry. There also exist some differences in the $S_1/S_0(3)$ and S_1 structure, as shown in Figure 1. With respect to the S_1 minimum, the $S_1/S_0(3)$ intersection has an energy of 31.1 kcal/mol at the CAS(8,7)/cc-pVDZ level of theory. Relatively large differences in structure and energy between $S_1/S_0(3)$ and S_1 predict that internal conversion (IC) to S_0 through the $S_1/S_0(3)$ intersection occurs with little possibility upon photoexcitation to the S_1 state of CH_3CONH_2.

D. The Most Probable Mechanism to Different Photoproducts. Photoexcitation at 220−270 nm leads to the CH_3CONH_2 molecules in the S_1 state. From this state, the CH_3CONH_2 molecules can relax via three nonradiative channels, besides radiation decay. They are internal conversion (IC) to the ground state, ISC to the T_1 state, and direct dissociation along the S_1 pathway. As pointed out before, the S_1/T_1 intersection is about 3.5 kcal/mol above the S_1 minimum. When the S_1 excess energy is less than 4 kcal/mol (∼110 kcal/mol above the S_0 minimum), the ISC to T_1 and the S_1 direct dissociations are inaccessible in energy, and the IC to S_0 should be the dominant nonradiative route, leading to hot parent molecules (S_0*). The decarbonylation reaction in the ground state has a barrier higher than 100 kcal/mol, and the S_0 C−C and C−N dissociations are endothermic by more than 80 kcal/mol, while the barrier height on the rate-determinant step of the dehydration is about 70 kcal/mol in the ground state. Thus, dehydration is the energetically favorable pathway after IC to the hot ground state. The mechanism of photoinduced dehydration of CH_3CONH_2 can be represented as $S_0 + h\nu \rightarrow S_1 \rightarrow$ IC $\rightarrow S_0^* \rightarrow TS1(S_0) \rightarrow IM(S_0) \rightarrow TS2(S_0) \rightarrow CH_3CN + H_2O$.

On the S_1 surface, the C−C bond fission is not in competition with the C−N bond dissociation that has a barrier of 9.5 kcal/mol. With the excess energy of 4−10 kcal/mol above the S_1 origin (110−115 kcal/mol above the S_0 minimum), the C−N bond fission is nearly inaccessible in energy, but the ISC to T_1 proceeds with high efficiency. In this energy range, the $S_1 \rightarrow T_1$ ISC process becomes a predominant route, and the decarbonylation reaction proceeds with little probability, due to a very high barrier on the T_1 pathway. Considering that the T_1 dehydration is a two-step process, and has a relatively high barrier (∼120 kcal/mol above the S_0 minimum) to the rate-determining step, the dehydration is not competitive with the C−C and C−N bond fissions on the T_1 surface. The CH_3CONH_2 molecules that relax to the T_1 state are left with enough internal energies to overcome the barriers to the C−C and C−N bond fissions. However, the T_1 C−N bond fission has a large preference over the C−C bond cleavage, because the former has a barrier of about 3.4 kcal/mol that is much lower than that of 12.0 kcal/mol for the latter.

The secondary dissociation of CH_3CO produced by the primary C−C, C−O, or C−Cl bond cleavage in CH_3COCH_3, CH_3COOH, or CH_3COCl has been extensively investigated from both experimental and theoretical viewpoints.[32,46−49] The energy barrier for the dissociation of CH_3CO into $CH_3 + CO$ has been estimated to be 17 kcal/mol. Once the CH_3CO radical is formed by the T_1 dissociation of CH_3CONH_2, the radical has sufficient internal energy to overcome the energy barrier, dissociating to CH_3 and CO. Actually, CH_3, CO, and NH_2 have been observed in the gas-phase photolysis[2] of CH_3CONH_2. A mechanism, $CH_3CONH_2(S_0) + h\nu \rightarrow CH_3CONH_2(S_1) \rightarrow$ ISC $\rightarrow CH_3CONH_2(T_1) \rightarrow TS_{C-N}(T_1) \rightarrow CH_3CO + NH_2 \rightarrow CH_3 + CO + NH_2$, can be used to illustrate the observed photoinduced decarbonylation behavior of CH_3CONH_2.

The CH_3CONH_2 molecules are populated in S_1 by photoexcitation at 248−220 nm, and the excited molecules have energy above the threshold of the direct S_1 C−N dissociation. In this case, the C−N bond cleavage can occur along the S_1 pathway. As pointed out before, the S_1/T_1 intersection is 3.5 kcal/mol above the S_1 minimum, while the top of the barrier for the C−N bond fission is 11.3 kcal/mol with respect to the S_1 minimum. The $S_1 \rightarrow T_1$ ISC process is favorable in energy, in comparison to the direct S_1 dissociation. It should be noticed that the ISC is a spin-forbidden process, which has a probability factor less than 1. If the spin-forbidden process is treated as a spin-allowed process, the rate calculated with the adiabatic RRKM theory will be reduced significantly. In view of energy and spin-forbidden effects, the direct S_1 C−N bond dissociation can compete with the $S_1 \rightarrow T_1$ ISC process upon photoexcitation at 230 nm and becomes predominant at a shorter wavelength.

Mechanisms for the $HCONH_2$ and $CH_3CONHCH_3$ photodissociations in the wavelength range of 220−270 nm are determined to be the same as that for CH_3CONH_2. Cleavage of the C−H or C−C bond α to the carbonyl group has nearly the same barrier height for $HCONH_2$, CH_3CONH_2, and $CH_3CONHCH_3$. The barrier to the α C−N fission is slightly higher for $CH_3CONHCH_3$ than for $HCONH_2$ and CH_3CONH_2. Early experiments[2] have found that substitution of a methyl group on the nitrogen atom in $HCONH_2$ and CH_3CONH_2 does not change the mechanism of photolysis of peptide bonds, but has a little influence on the relative rate of different dissociation channels.

(46) Shibata, T.; Li, H.; Katayanagi, H.; Suzuki, T. *J. Phys. Chem. A* **1998**, *102*, 3643.
(47) Owrutsky, J. C.; Baronavski, A. P. *J. Chem. Phys.* **1999**, *110*, 11206.
(48) Sumathi, R.; Chandra, A. K. *J. Chem. Phys.* **1993**, *99*, 6531.
(49) Deshmukh, S.; Myers, J. D.; Xantheas, S.; Hess, W. P. *J. Phys. Chem.* **1994**, *98*, 12535.

4. Summary

The S_0 and T_1 potential energy surfaces for $HCONH_2$, CH_3CONH_2, and $CH_3CONHCH_3$ dissociations have been mapped with the B3LYP and MP2 methods with the cc-PVDZ and cc-PVTZ basis sets, while the S_1 potential energy profile was determined by the CAS(8,7)/cc-PVDZ optimization followed by CASSCF/MRSDCI single-point calculations. The wavelength-dependent mechanisms were predicted through the computed potential energy surfaces and the surface crossing points. After the CH_3CONH_2 molecules are populated in S_1 by photoexcitation, there are three possible radiationless routes for CH_3CONH_2 to deactivate, internal conversion to the ground state, intersystem crossing to the lowest triplet state, and direct dissociation along the S_1 surface. When the S_1 excess energy is less than 4 kcal/mol, the dominant route is IC to S_0 followed by dehydration in the ground state. With an excess energy of 4−10 kcal/mol above the S_1 origin, the $S_1 \rightarrow T_1$ ISC process becomes a predominant route. The CH_3CONH_2 molecules that relax to the T_1 state are left with enough internal energies to overcome the barriers to the C−C and C−N bond fissions. However, the T_1 C−N bond fission has a large preference over the C−C bond cleavage. The CH_3CO radical formed by the T_1 C−N bond fission can further dissociate into CH_3 and CO. This is the most probable mechanism leading to formation of carbon monoxide. At the excitation energy above the threshold of the direct S_1 C−N dissociation, the $S_1 \rightarrow T_1$ ISC is in competition with the direct S_1 dissociation that overcomes the $TS_{C-N}(S1)$ barrier and then funnels through the $S_1/S_0(2)$ point down to either the hot parent molecule or the fragments of $CH_3CO + NH_2$ in the ground state. The mechanism that rationalizes the observed photochemical behavior of CH_3CONH_2 is predicted as follows:

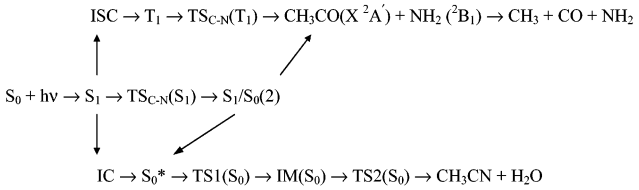

The same mechanisms of photodissociations were found for $HCONH_2$ and $CH_3CONHCH_3$. The methyl substitution on the nitrogen atom only has a little influence on the relative rate of different dissociation channels.

Acknowledgment. This work has been supported by the National Natural Science Foundation of China (Grant Nos. 20073005 and 20233020) and the Ministry of Science and Technology of China (Grant No. 2002CB613406).

Supporting Information Available: Structures and energies of the stationary points on the S_0, T_1, and S_1 surfaces for $HCONH_2$, CH_3CONH_2, and $CH_3CONHCH_3$ (PDF). This material is available free of charge via the Internet at http://pubs.acs.org.

JA029005H